ORIGINAL PAPER
LASER & PHOTONICS REVIEWS
www.lpr-journal.org

Deep Learning Enabled Laser Speckle Wavemeter with a High Dynamic Range

Roopam K. Gupta, Graham D. Bruce, Simon J. Powis, and Kishan Dholakia*

The speckle pattern produced when a laser is scattered by a disordered medium has recently been shown to give a surprisingly accurate or broadband measurement of wavelength. Here it is shown that deep learning is an ideal approach to analyze wavelength variations using a speckle wavemeter due to its ability to identify trends and overcome low signal to noise ratio in complex datasets. This combination enables wavelength measurement at high precision over a broad operating range in a single step, with a remarkable capability to reject instrumental and environmental noise, which has not been possible with previous approaches. It is demonstrated that the noise rejection capabilities of deep learning provide attometre-scale wavelength precision over an operating range from 488 nm to 976 nm. This dynamic range is six orders of magnitude beyond the state of the art.

1. Introduction

A key property of monochromatic optical waves is their wavelength. An accurate measurement of wavelength can enable many studies in fluorescence spectroscopy, atomic physics, and high precision metrology.[1,2] A standard wavemeter has a limitation of a one-dimensional dispersion. Using a dispersive element such as a diffraction grating can provide high bandwidth but resolution scales linearly with system size, whereas stabilized Fabry–Perot cavities can obtain high precision over a narrow operating range.[3] Recently, it has been recognized that speckle, which is the granular interference pattern produced when light propagates through a disordered medium, can overcome these limitations by multiplexing spatial-to-spectral mapping in a compact system. Tracking changes in this speckle pattern allows wavelength measurement with high resolution or broad operating range.[4] For wavelength measurement, speckle may be generated by passing light through either a multi-mode fibre[5–10] or into an integrating sphere.[11,12]

Capturing the speckle is insufficient: the critical step relies on the interpretation and understanding of the variation in speckle pattern as a function of wavelength. Without the detailed knowledge of the details of laser beam and medium, it is not generally possible to write a mathematical expression for the dependence of the speckle pattern on the wavelength. Instead, the extraction of wavelength must be accomplished by a data–driven approach in which a training phase uses a set of speckle images obtained at known wavelengths to identify the dependence of speckle on wavelength. Most of the previous applications use a method of calculating the transmission matrix of the given disordered medium,[13] and this gives the capability to measure wavelength over a range restricted solely by the sensitivity range of the camera used to image the speckle. However, the resolution of this method is limited by a high degree of correlation between the speckle patterns produced at closely-separated wavelengths,[14] typically on the picometre-scale. Multivariate analysis, in particular principal component analysis (PCA), adds a new dimension to this methodology and has allowed attometre-resolved wavelength measurements.[9] However, PCA allows for only a limited range of operation that has been demonstrated to be, at most, five orders of magnitude higher than the resolution.[11] Whilst these results are impressive, to truly convert speckle into a very precise measurement, a powerful single-step algorithm would be desirable. The speckle patterns generated after transmitting light through a disordered medium are unique for each wavelength, with the presence of inherent noise due to environmental or instrumental variations. As a consequence, speckle is likely to be an ideal candidate for the training of a deep learning based classification method.[15]

Deep learning is a powerful technique which has provided major advances in many areas of sciences, from evolutionary biology to quantum physics.[16,17] Particularly, deep learning based artificial neural networks (ANNs) automatically learn to identify and extract the relevant features present in an input dataset.[18] Moreover, the methodology for the application of ANNs makes

R. K. Gupta, Dr. G. D. Bruce, Prof. K. Dholakia
SUPA
School of Physics and Astronomy
University of St. Andrews
KY16 9SS, UK
E-mail: rg211@st-andrews.ac.uk
R. K. Gupta, Dr. S. J. Powis
School of Medicine and Biomedical Sciences Research Complex
University of St. Andrews
KY16 9TF, UK
Prof. K. Dholakia
Department of Physics
College of Science
Yonsei University
Seoul 03722, South Korea

DOI: 10.1002/lpor.202000120

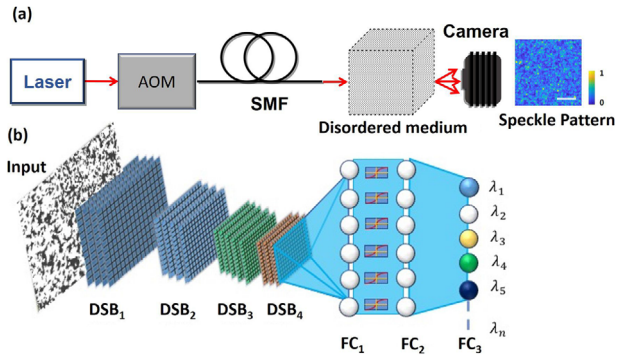

Figure 1. Speckle wavemeter assembly and CNN geometry. a) The experimental assembly for a speckle wavemeter. The laser wavelength is set using an acousto-optic modulator (AOM) and injected into the disordered medium via a single mode fibre (SMF). The output speckle pattern is captured by the camera. b) The convolutional neural network (CNN) used to classify the speckle images with respect to the incident laser wavelengths. The CNN consists of an input layer, multiple down-sampling blocks (DSB_i) and three fully connected layers (FC_i). Here λ_i denotes the output wavelength class. The white scale bar on the representative speckle pattern represents 224 μm, while the intensity is normalized as shown in the adjacent color bar.

them universal functional approximators[19] which are widely applied across physical sciences.[20–22] Deep learning based convolutional neural networks (CNNs) have already found application in speckle analysis for imaging applications.[23,24] Of particular relevance here, they have also been implemented to discriminate between different speckle-creating scatterers.[25] Additionally, harnessing the spectral characteristics of speckle, CNNs have found an application to achieve real-time recovery of hyperspectral information with a wavelength resolution of 5 nm.[26]

In this study, we present a method based on deep learning and t-distributed stochastic neighbor embedding (t-SNE)[27] to classify and segment the speckle images corresponding to a given laser wavelength. An interesting aspect presented in this study is the automatic rejection of instrumental or environmental noise by the CNN, which enables a classification of speckle patterns with a wavelength precision of two attometres, representing a nine orders of magnitude improvement compared to previous studies with deep learning.[26] This, coupled with the capability of the pre-trained CNN to segment the speckle images covering the entire visible spectrum, leads to a dynamic range improvement by six orders of magnitude. Going beyond the capability to identify the speckle-creating scatterer,[25] we additionally show that the trained CNN, in combination with t-SNE, can recognize the wavelength variations of speckle regardless of which scattering medium is used.

2. Experimental Section

The principle of the approach to measuring wavelength is outlined in **Figure 1**. The speckle patterns produced by scattering laser light from a disordered medium (Figure 1a) were recorded on a camera. Unless stated otherwise, a tunable diode laser which is wavelength-locked to a rubidium reference (~ 780 nm) was used as the source of laser light, an acousto-optic modulator to apply controlled wavelength variations, and an integrating sphere to scatter light.

To extract the wavelength dependence of the accumulated speckle images, a supervised deep learning based convolutional neural network (depicted in Figure 1b) was implemented.

2.1. Data Acquisition

The speckle images corresponding to the incident laser wavelength were generated by using a 1.5 inch diameter, spectralon integrating sphere. The laser light from an external cavity diode laser (Topica DL-100 / LD-0785-P220) was stabilized to the ^{87}Rb D2 line ($F = 2 \rightarrow F' = 2 \times 3$ crossover at ~ 780 nm) using saturated absorption spectroscopy and top-of-fringe locking. The light from the laser was passed through an acousto-optic modulator (AOM) (Crystal Technologies 3110-120) in a cat-eye double pass configuration to control the wavelength. Speckle is sensitive to many other laser parameters, including the polarization[28] and the transverse mode profile of the beam.[29–31] To ensure the variations in the speckle arise only from wavelength changes, the light was linearly polarized using a polarising beam splitting cube. To remove any variations in the spatial beam profile, the light was coupled into an angle cleaved single-mode fibre (SMF) (Thorlabs P5-780M-FC-10). This was connected to the integrating sphere input-port via an FC/PC connector without collimation optics to produce a diverging fundamental Gaussian mode within the integrating sphere. The SMF delivered 900 μW into the integrating sphere. The highly Lambertian diffusive coating and multiple reflections create large optical path differences allowing a high resolution for the system. As the generated speckle pattern also depends on the choice of observation plane, the light then propagated for a fixed distance of 20 cm before impinging the CMOS camera (Mikrotron EoSens 4CXP). This distance was chosen to achieve fully developed speckle patterns with a mean grain size of ~3 pixels (Figure 1a) to prevent sub-Nyquist sampling and associated aliasing effects.

To test the wavemeter over a broader range of the optical spectrum, additional lasers were used at wavelengths of 488 nm (M-Squared frequency-doubled SolsTis Ti:Sapphire), 532 nm (Oxxius single-longitudinal mode diode-pumped solid state laser), 671 nm (Thorlabs HL6756MG Diode Laser), and 976 nm (M-Squared SolsTis Ti:Sapphire). In order to test the generalization capabilities of the CNN, experiments were also performed by replacing the integrating sphere with a ground glass diffuser (Thoor-labs ED1-S20).

During the data accumulation, a continuous train of 10 000 128 × 128 pixel speckle images was recorded for each wavelength at a frame rate of 1 kHz with an exposure of 998 μs which took a total of 10 s. The time difference between the data accumulation of the different wavelength classes was typically 0.5 s.

2.2. Deep Learning Model Architecture, Training, and Calibration

To extract the wavelength dependence of the accumulated speckle images, a supervised deep leaning based convolutional neural network (CNN) (depicted in Figure 1b) was implemented. The implemented CNN architecture consisted of four down-sampling blocks (DSB). Each block consisted of three convolution layers

with 30 filters. Each convolution layer was followed by a batch normalization layer and a rectifier linear unit (ReLU) activation function layer. To systematically reduce the dimensionality of the input image, each DSB was connected with a max pooling layer with filter size of 2 px × 2 px. The filter sizes of convolution layers vary as 5 px × 5 px, 4 px × 4 px and 3 px × 3px, respectively, with a stride and padding of 1 px × 1 px. The DSBs were followed by two fully connected (FC) layers with leaky ReLU[32] as the activation function. Each FC layer with 128 neurons was followed by a dropout layer.[33] These layers were then fully connected to the output layer having n neurons with softmax activation function, here n denotes the number of wavelength classes. For attaining maximum classification accuracy over the validation dataset, the above-mentioned architecture was chosen after optimizing: the number of DSBs on the range 1–10; the number of convolution layers between 1 and 5 for each block; the filter sizes from 1 px × 1 px to 8 px × 8 px; and the number of neurons from 8 to 512 by doubling the neurons at each step.

The CNN geometry was optimized by considering the first dataset comprising the speckle images corresponding to 30 different wavelengths at a deviation of 2 fm. This dataset was randomly sampled into 70% training, 15% validation and 15% testing images corresponding to each wavelength. The training was implemented in Matlab 2018a over Nvidia Quadro P5000 GPU. To remove any intensity dependent fluctuations, all the speckle images were zero-center normalized. The CNN was trained to minimize the cross entropy cost function

$$\text{Cost} = -\frac{1}{k}\Sigma_x[y \times \log a + (1-y) \times \log(1-a)], \quad (1)$$

for 10 epochs in the mini batches of 128 images using an ADAM optimizer,[34] where Σ_x represents training over all the input images x, k is the total number of training data points, y is the target output and a is the network output. Here y and a are the one hot vectors representing the category of the input image. Initial learning rate was set at 1×10^{-6} and L2 regularization at 2×10^{-4}. The training process was validated after every 100 iterations.

During the training, the CNN learns to generalize the wavelength-dependent variations of the speckle patterns and thus classify them. The complete CNN architecture can be considered as composed of two ANNs, namely a convolution network (input layer to FC_1) and a classifier network (FC_2 and FC_3). The primary function of the convolution network is to down-sample the 2D input image into a 1D descriptor vector by filtering out the irrelevant / noisy features, whereas the classifier network is trained to classify these 1D descriptor vectors. Thus for a given time instant, where the speckle field is constant with respect to the environmental fluctuations, the convolution network learns to produce a 1D descriptor vector (128 px) corresponding to a particular wavelength for the input 2D image (128 × 128 px). Hence, after training, the vector output of the convolution network can be directly considered for further analysis.

2.3. t-SNE Analysis

To visualize the convolution network's segmentation capabilities over the different datasets, t-SNE was implemented over the generated 1D vectors. t-SNE is a well known non-linear method of machine learning which works on the principle of embedding a low dimensional space such that the neighborhood probabilistic distribution of the higher dimensional data is preserved in the low dimensional vector space. This was achieved by minimizing the symmetric form of Kullback–Leibler divergence.[27] In this study, t-SNE analysis with a perplexity of 30, was implemented using MATLAB 2018b.

3. Results

In this section, we present the capabilities of deep learning to measure wavelength deviation from the speckle pattern. Following the training and optimization of the CNN geometry, we identified the limit of detection by showing attometre-scale wavelength precision, a broadband operation range of the CNN based speckle wavemeter, and explored the generalization capabilities of the CNN by changing the disordered medium.

3.1. CNN Optimization

For the optimization and calibration of the CNN, we varied the wavelength in 2 fm steps over a range of 60 fm. The complete dataset consisted of 10 000 images corresponding to each wavelength, which were randomly divided into training, validation, and test datasets by the fraction of 70%, 15%, and 15% respectively. To calibrate the CNN, training is performed using every image in the training set.

During the training, a global error is computed by parsing a batch of images sampled randomly from each class of the training set. During the backward pass, this calculated error is backpropagated such that the network can identify the features representing each individual class. In this study, this process is implemented to optimize a CNN architecture over the femtometre-resolved speckle patterns for gaining maximum classification accuracy over the validation dataset.

After the training process, images from the test set (a total of 45 000 images across all the wavelengths) were considered for testing the performance of the CNN. The one-hot classification by the CNN led to a very accurate measurement with 100% classification accuracy. To evaluate the probabilistic classification error of the CNN we calculated the softmax output of the FC_3 layer for the test dataset. The error was calculated by taking the sum of all the incorrect classification values for each image and then taking the average of this summed value over all the images. This leads to a probabilistic classification error of 2.2×10^{-6}. To emphasize this fact, we calculated the confusion matrix from the softmax output of the CNN over $\log_{10}$ scale, which is presented in **Figure 2**. For the optimal architecture, the CNN classification accuracy does not depend on the number of training classes, or the step size between them.

3.2. CNN Noise Rejection Capabilities

It has been shown in a previous study that the CNN, once trained on a given dataset, learns to overcome a low signal to noise

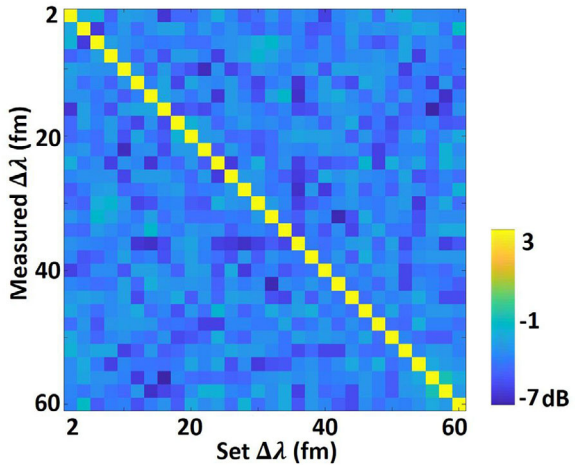

Figure 2. Demonstration of high-accuracy discrimination of femtometre-resolved wavelength changes. Confusion matrix for the output of the CNN in classifying speckle patterns corresponding to wavelength separations on the femtometre-scale, plotted on $\log_{10}$ scale. The color bar represents the decibel values.

environment.[35] In our study we find analogous results. Through the training process, the CNN learns to reject variations in the speckle patterns which do not correspond to the control parameter, that is, wavelength. This is demonstrated in **Figure 3**, where we analyzed the speckle images by implementing PCA on both the input raw images and the processed output of the CNN. To evaluate an improvement in the stability of the speckle image time series (accumulated for 1 second) before and after the CNN transformation (Figure 3b and d) we estimated the smallest detectable shift in wavelength to be three times the standard deviation (σ) from the mean position. The 3σ value of the first principal component (PC1) was evaluated as 0.014 for the raw speckle images whereas it was evaluated as 0.003 for the output of the CNN, an improvement by a factor of 4.66. Additionally, to analyze the periodic variations in the data, we calculated the Fourier transform of PC1 (Figure 3c,e). For the raw input speckle images at a fixed wavelength, PC1 of the input images show several periodic noise components. However, when the output of the convolution network (FC_1) is analyzed using PCA, PC1 does not reflect any of the temporal noise components that were present in the input dataset. This shows that the CNN, once trained to classify the speckle images with respect to wavelengths, filters the input speckle images and returns the output as a 1D vector representing a single wavelength without any environmental or instrumental noise.

Given the widely known capability of ANNs to operate as universal functional approximators,[19] the results in Figure 3d and 3e also orient us toward a conclusion that once the CNN is trained to classify the speckle images for a single wavelength, it processes the input images to down-sample them into one dimensional vector such that any noisy components are rejected. This suggests that we can further train the CNN to recognize the incident laser wavelength with a precision below the instrumental circuitary noise.

3.3. Attometre Precision

In order to observe the limit of detection of the trained deep learning model, we accumulated a second dataset where the laser wavelength was tuned over separations on the attometre scale. More specifically, the speckle images were captured by detuning the acousto-optic modulator across five distinct wavelengths with an increment of two attometres. The time taken to accumulate

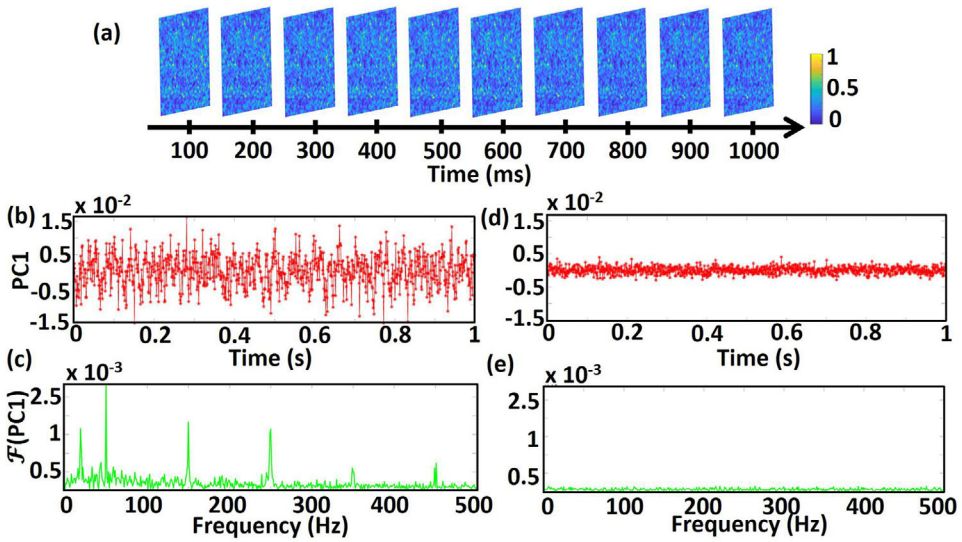

Figure 3. CNN-enabled noise rejection. The CNN learns, through training, to reject instrumental noise from the wavelength measurement. For an example dataset comprising 1000 images sampled over 1 second at a fixed wavelength, a) shows example speckle images captured at every 100 ms. The color bar represents normalized intensity. b) PC1 of the full train of speckle images and c) the Fourier transform of (b) identify the presence of continuous variations in the dataset. d) PC1 of the 1D descriptor vectors (which are the processed output of the CNN) and e) the Fourier transform of (d) highlight the absence of any variations present in the output of the CNN. Here, PC1 denotes the first principal component

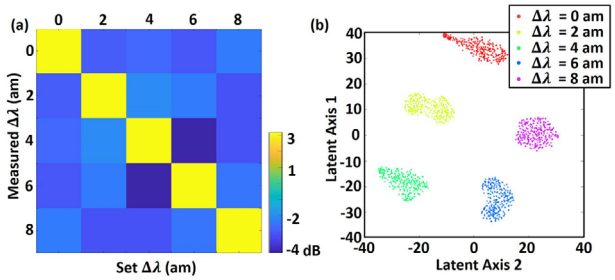

Figure 4. CNN classification and segmentation capabilities of attometre-resolved speckle data. a) Confusion matrix on the log_{10} scale depicting the classification abilities of the CNN for wavelengths separated by 2 am. Here $\Delta\lambda = 0$ am depicts a detuning of $\Delta\lambda = 30.652$ fm from the rubidium crossover and the other values are relative to it. The color bar represents the decibel values. b) t-SNE visualization for the output of the FC_1 from the CNN trained over femtometre-resolved speckle data, applied to speckle data separated by two attometres. The speckle images at each wavelength form a distinct cluster, showing that the CNN can be retrained simply by using a single speckle image at a known wavelength.

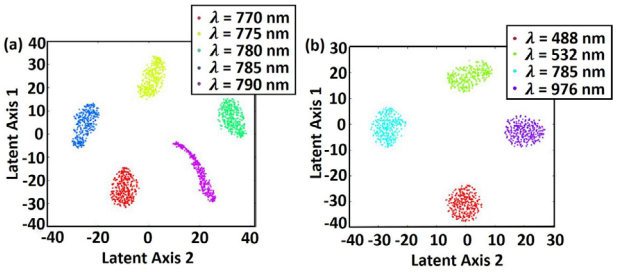

Figure 5. Segmentation capabilities of the CNN over a broadband range of data. a) t-SNE scatter plot of the output of the 1D descriptor vector for the wavelength deviations corresponding to 770, 775, 780, 785, and 790 nm. b) t-SNE scatter plot of the 1D descriptor vector corresponding to 488, 532, 785, and 976 nm.

the dataset for a single wavelength was 10 s whereas the time difference between the different wavelength classes was typically 0.5 s. This ensures that any wavelength drift between measurements should be small compared to the drift within a single measurement period. Moreover, we see no evidence of drift within the measurement period (see Figure 3), verifying that each measurement is congruent to a single wavelength.

As the dataset is changed, the classification abilities of the CNN needs to be re-tuned, hence by the virtue of transfer learning, we retrained the CNN by changing the number of neurons in the output layer (FC_3). A total of 7000 images per wavelength class were considered for training/validation and 3000 images per class were considered for the testing process. The retrained CNN gave a one-hot classification accuracy of 100% and a softmax probabilistic classification error of 3.8×10^{-5}. To emphasize the accuracy of measurement, we show the $\log_{10}$ of the confusion matrix in **Figure 4a**. This matrix was calculated from the activations of the softmax layer at the output of the trained CNN. These results show that the re-training of a CNN can result in a wavelength precision as low as 2 am. This wavelength precision of two attometres is not a fundamental limit, but limited by the precision with which we can control the wavelength using the AOM in the experiment.

To eliminate the process of retraining the CNN, the images were also processed using the CNN trained to classify the fm-resolved data. The output 1D vectors at FC_1 were further analysed using t-SNE (see Section 2 Subsection 2.3) to visualize the segmentation capabilities. Figure 4b denotes the output of FC_1 layer of the CNN downsampled to a two-dimensional latent vector space. Each cluster represents the speckle images corresponding to a specific wavelength. Evidently, using this method we do not need to train the CNN further using 7000 images per class but we can use only a single image for the further classification, and still achieve attometre-scale precision.

The resolving power of a wavemeter is $R = \frac{\lambda_0}{\delta\lambda}$, where λ_0 is the absolute wavelength and $\delta\lambda$ is the minimum detected deviation from it. The resolving power of the deep learning enabled speckle wavemeter is $R > 10^{11}$ for a central wavelength at 780 nm with a least deviation of 2 attometre.

3.4. Broadband Operation Range

We tested the broadband segmentation capabilities of the CNN by accumulating the speckle patterns over two wavelength ranges: from 770 nm to 790 nm in 5 nm increments and separately at 488 nm, 532 nm, 785 nm, and 976 nm (see Experimental Section for details).

When the fm-trained CNN was implemented over the two datasets, and the output of FC_1 was analyzed using t-SNE, the speckle images corresponding to individual wavelength were clustered independently as depicted in **Figure 5a,b**. With respect to the interpolative estimation, this result shows that once the CNN is trained, it can be harnessed for the classification of speckle images at a broadband range between 488 nm and 976 nm regardless of the variation in the incident laser wavelength.

As before, without retraining the CNN, t-SNE evaluation of the output of FC_1 shows a clear clustering of the classes, meaning that a full retraining is not necessary, but wavelength detection can be accomplished simply by using one known wavelength per cluster. The fractional bandwidth of the wavemeter is $B = (\lambda_{max} - \lambda_{min})/\frac{1}{2}(\lambda_{max} + \lambda_{min})$, where λ_{max} is the maximum detected wavelength and λ_{min} is the minimum detected wavelength in the broadband operation range, giving $B = 0.66$ for the speckle wavemeter presented here.

3.5. High Dynamic Range

Defining the dynamic range as the product $B \times R$, these results showcase the high dynamic range capability of the CNN in classifying the speckle patterns: identifying wavelength differences with a precision of a few attometres over a range of 100s of nanometres gives a high dynamic range of 3.25×10^{11}.

To display the high dynamic range capabilities of the CNN we also accumulated the data using diode lasers locked to the D2 lines of ^{87}Rb (~780 nm) and ^{7}Li (~671 nm). For each laser, we use the AOM to generate two set of speckle patterns, with a wavelength separation of 2 am between each of the two sets. This resulted in a broadband wavelength measurement with a precision of 2 am. As can be inferred from **Figure 6**, t-SNE plot shows the presence of four distinct clusters corresponding to the four mentioned wavelengths.

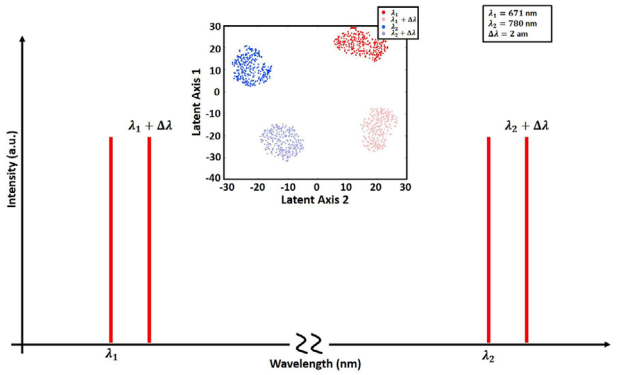

Figure 6. High dynamic range of the CNN. The graph visualizes the speckle patterns accumulated at four distinct wavelengths at 780 nm, 780 nm + $\Delta\lambda$, 671 nm and 671 nm + $\Delta\lambda$. The inset graph represents the t-SNE scatter plot of the output of the 1D descriptor vector for the mentioned wavelengths. (Here $\Delta\lambda$ = 2 am)

3.6. Generalization Capabilities of the CNN

The speckle pattern represents the spatial correlation function of a given disordered medium and the incident light wavelength. This means that if a different scattering medium is used, the speckle pattern would also be different but maintain the wavelength dependent deviations.[36] Therefore, with respect to the generalization capability, a deep learning based model trained to decorrelate the speckle patterns with respect to wavelength should in principle be able to segment the speckle images generated from any random disordered medium. To consider this theory of generalized segmentation properties, we accumulated a dataset using a ground glass diffuser (Thorlabs ED1-S20) in place of the integrating sphere. As can be observed from **Figure 7a,b**, the speckle patterns generated from the integrating sphere and the ground glass show completely different characteristic features.

We accumulated two sub-datasets, one where the speckle images were accumulated by varying the incident wavelength with an increment of 2 fm and the other with an increment of 20 am. The segmentation capability of the CNN, trained over femtometre resolved data, was tested by processing the speckle images generated from each class. The output from FC_1 was analysed using t-SNE and the results are presented in Figure 7. As shown in Figure 7c,d, the CNN segments and clusters each of the speckle images into their individual class.

The results clearly show that the CNN processed the images, which represented completely different spatial variations, and clustered them with respect to the incident laser wavelength.

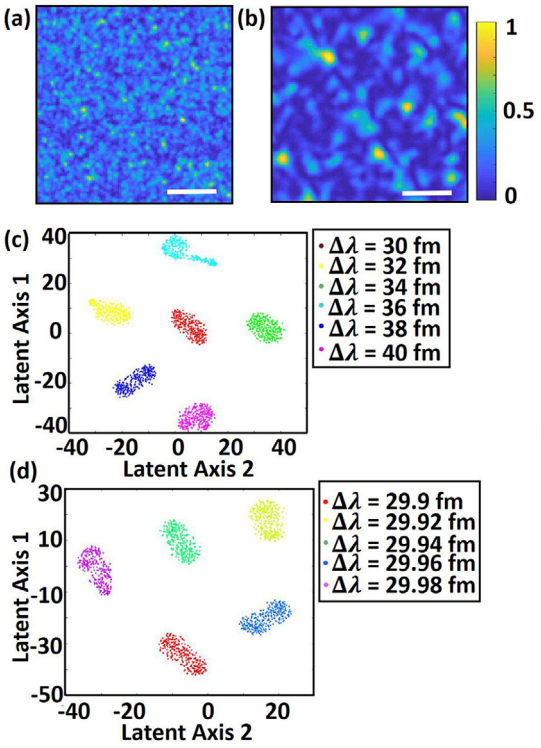

Figure 7. Transferring wavelength classification to a different scattering medium. Speckle pattern generated using an a) integrating sphere and b) ground glass assembly. The color bar represents normalized intensity while the white scale bar represents 224 μm. Segmentation results using ground glass assembly for c) femtometre-resolved and d) attometre-resolved incident laser wavelength modulations.

4. Discussion

The combination of speckle with CNNs achieves a remarkable classification accuracy since speckle patterns represent an ideal candidate for the training of the CNN. As shown in Figure 2, the CNN achieves a one-hot classification accuracy of 100%, with a softmax probabilistic classification error of 2.2×10^{-6}. If the disordered medium and the laser wavelength are kept constant then, ideally, the resulting speckle pattern should not change. However, the environmental fluctuations or fluctuations due to instrumental circuitry cause the speckle patterns to change with time. Therefore, we have also demonstrated that the CNN, once trained to classify the speckle patterns, automatically learns to reject the environmental or instrumental fluctuations.

As can be inferred from Figure 3, the structure of a CNN model and backpropagation training, drives it to progressively learn the filtering of the input images. As explained before, the training is implemented such that the output only contains the features relevant to the individual class of the images in the training dataset. In the case of a speckle wavemeter, conceptually, the speckle images should be down-sampled such that the output only contains the features with respect to the wavelength. In this study, we have demonstrated that the CNNs can accurately classify speckle patterns measured with a wavelength separation of 2 am (Figure 4) which can be attributed to the automated noise rejection capability of the CNN.

The results demonstrated in Figure 3, in combination with the universal function approximator property of the CNN, provide an insight that this model once trained can be implemented (in combination with a dimensionality reduction algorithm) to segment the wavelength-dependent speckle with any deviation and generated from any disordered media. The results presented in Figures 5–7 highlight these properties of the deep learning based model.

ANNs, although powerful tools, also come with potential limitations. When compared to other statistical methods, an ANN takes considerably more time for the training process. Moreover, for a classification problem, the training time increases exponentially with the number of classes. Additionally, the ANN which is trained to classify, can only identify data-points which are part of training set classes. This would apparently restrict the range and precision of the speckle wavemeter. Whilst a regression-based approach seems to be an attractive option to generalize over the unknown data-points, this generalization capability seems to be limited at a much lower precision.[37] Instead, this potential limitation has been overcome here by the application of t-SNE which enables relative wavelength measurement for speckle patterns which are not part of the training set classes.

5. Conclusion

In conclusion, this study has implemented a deep learning based method to classify the speckle patterns with respect to the incident light source wavelength. The combination of laser speckle and deep learning provides an accurate method to distinguish between laser wavelengths separated by as little as 2 am and as much as 488 nm, showing a dynamic range of 3.25×10^{11} in a single-step algorithm. This combination can also be applied to a completely distinct scattering medium, and re-calibrating the CNN using the method of transfer learning provides an efficient training procedure for a highly accurate wavemeter.

Additionally, this study shows that a trained deep learning model can be implemented to reject inherent instrumental or environmental noise. The results presented here will be beneficial in not only automated laser stabilization but may also be useful for noise reduction in multiple telecommunication applications. In the future, we will investigate extending this work to the development of robust and compact spectrometers with a capability to measure multiple wavelengths, and will also investigate the possibility to train the CNN to simultaneously measure wavelength, polarization, and transverse mode profile.

Acknowledgements

The authors would like to acknowledge technical assistance from Dr. Donatella Cassettari. This work was supported by a Medical Research Scotland Ph.D. studentship Ph.D. 873-2015 awarded to R.K.G, and grant funding from Leverhulme Trust (RPG-2017-197) and UK Engineering and Physical Sciences Research Council (grant EP/P030017/1). The opinions expressed in this article are the authors own and do not reflect the view of above mentioned funding agencies.

Conflict of Interest

The authors declare no conflict of interest.

Author Contributions

The experiments were designed by R.K.G., G.D.B., and K.D. R.K.G. developed and designed the CNN and performed the numerical analysis. G.D.B. developed the experimental setup and performed the experiments. K.D. and S.J.P. supervised the study. The manuscript was written by R.K.G. with contributions from G.D.B. and K.D. All authors approved the manuscript. Research data supporting this publication can be accessed at https://doi.org/10.17630/d6049ec8-972e-4820-9cd4-9552b26c8426

Keywords

automated noise rejection, deep learning, speckle metrology, wavelength measurement

Received: March 27, 2020
Revised: May 28, 2020
Published online:

[1] R. H. Leonard, A. J. Fallon, C. A. Sackett, M. S. Safronova, *Phys. Rev. A* **2015**, *92*, 052501.
[2] R. Erf, *Speckle Metrology*, Elsevier **2012**.
[3] M. Chakrabarti, M. L. Jakobsen, S. G. Hanson, *Opt. Lett.* **2015**, *40*, 3264.
[4] H. Cao, *J. Opt.* **2017**, *19*, 060402.
[5] B. Redding, H. Cao, *Opt. Lett.* **2012**, *37*, 3384.
[6] B. Redding, S. M. Popoff, H. Cao, *Opt. Express* **2013**, *21*, 6584.
[7] B. Redding, M. Alam, M. Seifert, H. Cao, *Optica* **2014**, *1*, 175.
[8] N. H. Wan, F. Meng, T. Schröder, R. J. Shiue, E. H. Chen, D. Englund, *Nat. Commun.* **2015**, *6*, 7762.
[9] G. D. Bruce, L. O'Donnell, M. Chen, K. Dholakia, *Opt. Lett.* **2019**, *44*, 1367.
[10] G. D. Bruce, L. O'Donnell, M. Chen, M. Facchin, K. Dholakia, *Opt. Lett.* **2020**, *45*, 1926.
[11] N. K. Metzger, R. Spesyvtsev, G. D. Bruce, B. Miller, G. T. Maker, G. Malcolm, M. Mazilu, K. Dholakia, *Nat. Commun.* **2017**, *8*, 15610.
[12] L. O'Donnell, K. Dholakia, G. D. Bruce, *Opt. Commun.* **2020**, *459*, 124906.
[13] S. M. Popoff, G. Lerosey, R. Carminati, M. Fink, A. C. Boccara, S. Gigan, *Phys. Rev. Lett.* **2010**, *104*, 100601.
[14] M. Mazilu, T. Vettenburg, A. Di Falco, K. Dholakia, *Opt. Lett.* **2014**, *39*, 96.
[15] Y. Bengio, A. Courville, P. Vincent, *IEEE Transactions on Pattern Analysis and Machine Intelligence* **2013**, *35*, 1798.
[16] J. F. Hoyal Cuthill, N. Guttenberg, S. Ledger, R. Crowther, B. Huertas, *Sci. Adv.* **2019**, *5*, eaaw4967.
[17] M. Schuld, N. Killoran, *Phys. Rev. Lett.* **2019**, *122*, 040504.
[18] R. K. Gupta, M. Chen, G. P. A. Malcolm, N. Hempler, K. Dholakia, S. J. Powis, *Opt. Express* **2019**, *27*, 13706.
[19] K. Hornik, M. Stinchcombe, H. White, *Neural Networks* **1989**, *2*, 359.
[20] P. Baldi, P. Sadowski, D. Whiteson, *Nat. Commun.* **2014**, *5*, 4308.
[21] B. S. Rem, N. Käming, M. Tarnowski, L. Asteria, N. Fläschner, C. Becker, K. Sengstock, C. Weitenberg, *Nat. Phys.* **2019**, *15*, 917.
[22] H. Wang, Y. Rivenson, Y. Jin, Z. Wei, R. Gao, H. Günaydın, L. A. Bentolila, C. Kural, A. Ozcan, *Nat. Methods* **2019**, *16*, 103.
[23] R. Horisaki, R. Takagi, J. Tanida, *Appl. Opt.* **2018**, *57*, 3859.
[24] Y. Li, Y. Xue, L. Tian, *Optica* **2018**, *5*, 1181.
[25] E. Valent, Y. Silberberg, *Optica* **2018**, *5*, 204.
[26] U. Kürüm, P. R. Wiecha, R. French, O. L. Muskens, *Opt. Express* **2019**, *27*, 20965.
[27] L. van der Maaten, G. Hinton, *J. Mach. Learn. Res.* **2008**, *9*, 2579.
[28] M. Facchin, G. D. Bruce, K. Dholakia, *OSA Continuum* **2020**, *3*, 1302.
[29] A. Mourka, M. Mazilu, E. M. Wright, K. Dholakia, *Sci. Rep.* **2013**, *3*, 1422.

[30] S. G. Reddy, S. Prabhakar, A. Kumar, J. Banerji, R. Singh, *Opt. Lett.* **2014**, *39*, 4364.
[31] X. B. Hu, M. X. Dong, Z. H. Zhu, W. Gao, C. Rosales-Guzmán, *Sci. Rep.* **2020**, *10*, 199.
[32] A. L. Maas, A. Y. Hannun, A. Y. Ng, Rectifier Nonlinearities Improve Neural Network Acoustic Models, in: Proc. ICML, (**2013**), p. 3.
[33] N. Srivastava, G. Hinton, A. Krizhevsky, I. Sutskever, R. Salakhutdinov, *J. Mach. Learn. Res.* **2014**, *15*, 1929.
[34] D. P. Kingma, J. Ba, Adam: A method for stochastic optimization, in: 3rd International Conference on Learning Representations, ICLR 2015, San Diego, CA, USA, May 7-9, 2015, Conference Track Proceedings, (**2015**).
[35] S. Helgadottir, A. Argun, G. Volpe, *Optica* **2019**, *6*, 506.
[36] N. George, A. Jain, *Appl. Phys.* **1974**, *4*, 201.
[37] E. B. Magnusson, J. P. B. Mueller, M. Juhl, C. Mendoza, K. Leosson, *ACS Photonics* **2018**, *5*, 2682.